ADVANCED BIOSYSTEMS
www.adv-biosys.com

Enhanced Cellular Transduction of Nanoparticles Resistant to Rapidly Forming Plasma Protein Coronas

*Lia A. Blokpoel Ferreras, Daniel Scott, Saul Vazquez Reina, Paul Roach, Teobaldo E. Torres, Gerardo F. Goya, Kevin M. Shakesheff, and James E. Dixon**

Nanoparticles (NPs) are increasingly being developed as biomedical platforms for drug/nucleic acid delivery and imaging. However, in biological fluids, NPs interact with a wide range of proteins that form a coating known as protein corona. Coronae can critically influence self-interaction and binding of other molecules, which can affect toxicity, promote cell activation, and inhibit general or specific cellular uptake. Glycosaminoglycan (GAG)-binding enhanced transduction (GET) is developed to efficiently deliver a variety of cargoes intracellularly; employing GAG-binding peptides, which promote cell targeting, and cell penetrating peptides (CPPs) which enhance endocytotic cell internalization. Herein, it is demonstrated that GET peptide coatings can mediate sustained intracellular transduction of magnetic NPs (MNPs), even in the presence of serum or plasma. NP colloidal stability, physicochemical properties, toxicity and cellular uptake are investigated. Using label-free snapshot proteomics, time-resolved profiles of human plasma coronas formed on functionalized GET-MNPs demonstrate that coronae quickly form (<1 min), with their composition relatively stable but evolving. Importantly GET-MNPs present a subtly different corona composition to MNPs alone, consistent with GAG-binding activities. Understanding how NPs interact with biological systems and can retain enhanced intracellular transduction will facilitate novel drug delivery approaches for cell-type specific targeting of new nanomaterials.

1. Introduction

Nanoparticles (NPs) are broadly used in biomedical and biotechnological applications due to their physical properties.[1] Their small size and high surface area makes NPs ideal carriers (for example, for macromolecular nucleic acids and small molecule drugs), and magnetic variants (magnetic NPs; MNPs) have physical properties suitable for directly targeting therapeutic sites using magnetic fields.[2] Furthermore, the ability of MNPs (a subtype being superparamagnetic iron oxide NPs; SPIONs) to efficiently convert magnetic energy into thermal energy, makes them a focus of interest for use in hyperthermia-based cell ablation anticancer therapies (such as Magforce Nanotechnologies AG).[3–6] Other relevant applications include imaging (including a focus on regenerative medicine), tissue engineering, for mechanical stimulation for cell differentiation in vivo[7–17] and, most recently, their use as synthetic enzymes in biocatalytic processes.[18]

Targeted delivery strategies for MNPs have been developed toward specific- or overexpressed receptors on diseased cells by functionalizing the NP surface with proteins, antibodies, or other biomolecules as targeting ligands. These strategies efficiently enhance NP delivery to the target cells in vitro; however, there is mounting evidence that targeting ability of functionalized NPs disappears when placed in an in vivo biological environment.[19–21]

It is now well established that when any material surface encounters a biological system, interactions occur between the material and the system components (i.e. proteins, lipids, DNA) forming a layer termed the protein corona. The protein corona defines the biological identity of the particle or surface, and has proven to be an obstacle in the past for effective targeted delivery of ligands, since it affects the physicochemical

Dr. L. A. Blokpoel Ferreras, Prof. K. M. Shakesheff, Dr. J. E. Dixon
Regenerative Medicine and Cellular Therapies Division
The University of Nottingham Biodiscovery Institute (BDI)
School of Pharmacy, University of Nottingham
Nottingham NG7 2RD, UK
E-mail: james.dixon@nottingham.ac.uk

The ORCID identification number(s) for the author(s) of this article can be found under https://doi.org/10.1002/adbi.202000162.

DOI: 10.1002/adbi.202000162

Dr. D. Scott
School of Life Sciences, University of Nottingham
Nottingham NG7 2RD, UK

S. Vazquez Reina
School of Veterinary Sciences
University of Nottingham
Nottingham NG7 2RD, UK

Dr. P. Roach
Department of Chemistry
Loughborough University
Leicestershire LE11 3TU, UK

Dr. T. E. Torres, Prof. G. F. Goya
Institute of Nanoscience of Aragón
University of Zaragoza
50009, Zaragoza, Spain

properties of the particles and the availability of targeted ligand interaction.[22–26]

We have developed a peptide-based system, which can be grafted onto the surface of MNPs, specifically here dextran-coated SPIONs. This system is termed glycosaminoglycan (GAG)-binding enhanced transduction (GET) and its efficiency relies on the synergistic combination of a cell penetrating peptide (CPP) and a membrane docking peptide to heparan sulfate GAGs.[27] Importantly, we have demonstrated that these peptides can be employed to deliver MNPs in vitro,[9,27] can be used in vivo for gene therapy,[28,29] and for delivering recombinant proteins for tissue engineering applications.[30–32]

In this study, we have characterized and quantified the physicochemical properties and delivery of GET peptide-coated MNPs (GET–MNPs) to mammalian cells in vitro. GET electrostatic coating (we term "complexation") was able to efficiently enhance particle uptake in protein-free, and in serum and plasma-rich conditions. As this appeared to conflict with published examples that use cell membrane targeting of NPs,[19–21] we investigated the structure and complexity of our MNP interface within these biological microenvironments. We examined protein corona density and complexity formed on GET–MNPs over time as well as any pathobiological effects. We demonstrate that GET–MNPs are resistant to the inhibitory effect of serum- or plasma-coronas, suggesting that our system can be used in such complex biological microenvironments for application of nanotechnology. Furthermore, the complexity of the coronae can be linked to the GET peptides ability to interact with GAG-associated proteins, and there were no apparent effects on hemotoxicity. Our study therefore is significant in understanding how protein–particle interactions can affect targeting, uptake, and biocompatibility when exploiting nanotechnologies for nanomedicine.

2. Results

2.1. Facile Production of Monodispersed Electrostatically Coupled GET-Coated MNPs

Currently, dextran-coated MNPs or SPIONs (containing iron oxide cores) are being translated for a wide number applications in biomedicine.[7,33–35] We employed commercially available dextran-COOH-coated SPIONS (Nanomag-D, 250 nm, Micromod) for these studies. These particles can be captured by use of a static magnet and have been previously used for hyperthermia-mediated cell death and cell tracking in vivo.[9,36] Transmission electron microscopy (TEM) analysis of MNPs in the colloidal dispersion showed a multicrystallite structure of the NPs, having irregular shape and average size of 133 nm ± 38 nm (**Figure 1**a; Figure S1, Supporting Information). Thermogravimetric analysis (TGA) showed a percentage of organic phase of 24.4 ± 2.4%, confirming the presence of dextran in the particles (Figure S2 and Table S1, Supporting Information). Data obtained with these MNPs was highly reproducible, negating the often confounding factor of heterogeneity in commercially obtained MNPs. As we were confident in the source and properties of these MNPs, we employed them throughout our studies. Previously, we have shown that by simple co-incubation of GET peptides with these MNPs, we could enhance intracellular uptake of MNPs into mammalian cells.[9,27] Our system relies on electrostatic interaction of the positive GET peptides and negative cargo for nucleic acid delivery applications.[27–29] These dextran-coated MNPs are negatively charged and therefore hypothesized to directly interact with GET peptides through electrostatic binding. The GET peptide, P21-8R (Figure 1b), is a positively charged L-amino acid (isoelectric point pI ≈12),[27] so in order to confirm electrostatic interactions between GET and MNPs, we studied the zeta potential of MNPs at increasing GET concentrations (Figure 1c). The shift in zeta potential of MNPs (−26.2 mV) compared with GET functionalized particles at 4 and 8 nmol mg^{-1} (11.7 and 20.3 mV, respectively) indicates strong electrostatic interaction between the dextran-coated particles and the positively charged GET, which was proportional to the peptide's concentration. Dynamic light scattering (DLS) analysis showed particles in the monodisperse range after functionalization with 4–8 nmol mg^{-1} of GET (Figure 1d and **Table 1**) with no significant changes from particle size distribution compared to noncomplexed MNPs.[37]

2.2. GET Peptides Are Absorbed to MNPs and Change Conformation

Upon adsorption onto a surface, protein molecules can experience a change in conformation and/or orientation in search of the most energetically stable arrangement. Driven by hydrophobicity and charged group interaction these structural changes can impact on protein–substrate interactions and thereby reduce their availability/bioactivity.[38–40] It was therefore paramount to understand the degree of change in the peptide structure upon adsorption. Protein structure can be studied through the analysis of their amide I band, which provides a very strong adsorption by infrared spectroscopy. This band can be deconvoluted in order to quantify secondary structure components (Figure S3, Supporting Information).[41–43] GET significantly loses alpha-helical structure in favor of beta-sheet component (alpha-helix fraction decreases from 0.26 to 0.22, $p < 0001$, $n = 9$; beta-sheet fraction increases 0.29 to 0.32, $p < 0.0001$, $n = 9$). These changes suggest a certain degree of denaturation of the original GET peptide secondary structure on interaction with MNPs. The increase of beta-sheet component suggests a higher coordination of the different subunits of the molecule (containing the lysine-rich P21 peptide GAG-binding domain and octo-arginine 8R CPP component). A change in structure toward beta-sheet at the expense of alpha-helix has been observed by others investigating protein–NP interaction,[43] highlighting the structural change in association with the MNPs surface. The differences on GET secondary structure when incubated with MNPs further reinforce the DLS and zeta potential data in confirming the direct interaction of the GET peptide with MNPs.

The complexity of any protein adsorption process makes development of models that account for all the possible

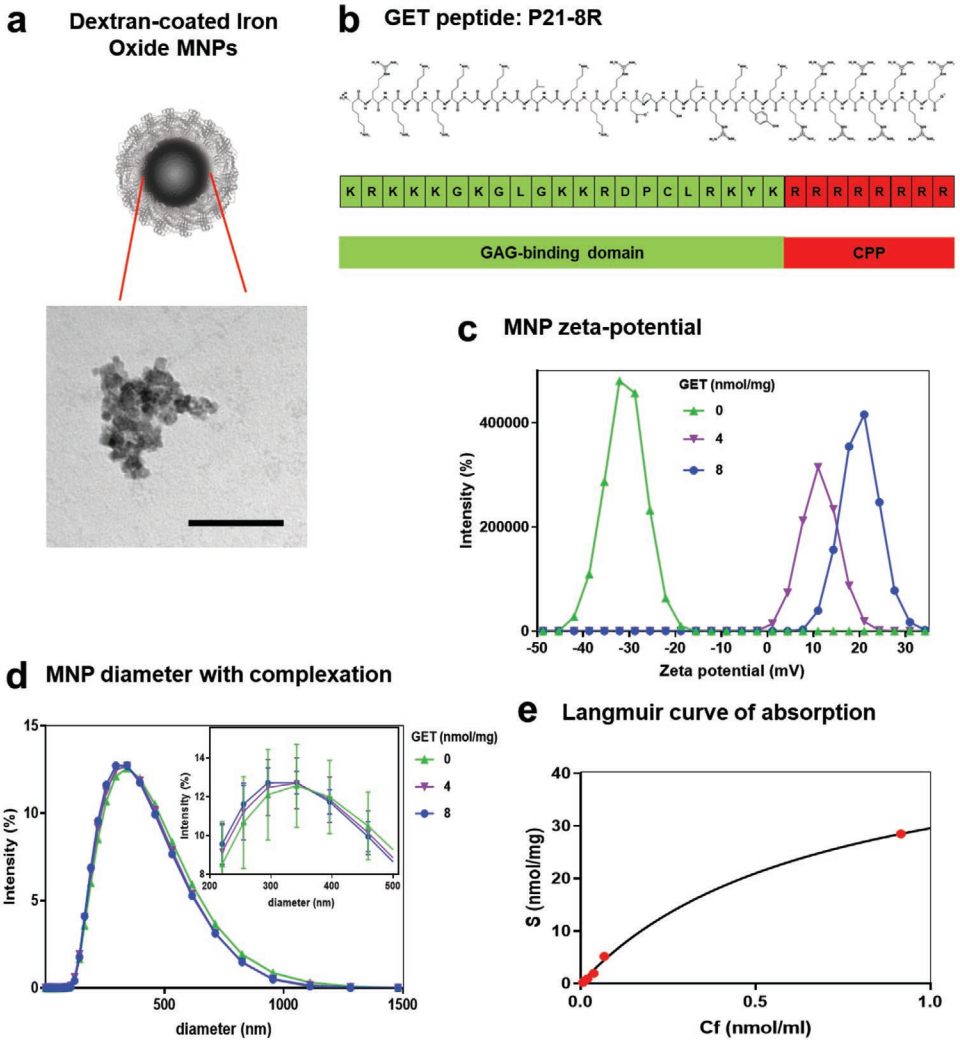

Figure 1. GET peptides bind to MNPs through electrostatic interaction. a) Representative TEM image of the Micromod Nanomag-D 250 nm particles (MNPs) showing the size of the magnetic core is about 100 nm in diameter. Scale bar: 100 nm. b) GET peptide, P21-8R, primary structure, and amino acid sequence. GAG-binding domain represented in green and cell penetrating peptide domain (CPP) represented in red. c) Zeta potential distribution of particles 50 µg incubated with increasing concentrations of GET (GET concentration expressed as nmol GET mg^{-1} of particles). Zeta potential was measured in water. The shift in zeta potential indicates the interaction of GET with MNPs (n = 6 independent repeats, 3 subruns per repeat). d) Apparent diameter of the particles obtained by DLS for 50 µg mL^{-1} of MNPs incubated with increasing concentrations of GET (GET concentration expressed as nmol GET mg^{-1} of particles). DLS measurements were done in water (n = 6 independent repeats, 3 subruns per repeat, error bars in the close-up plot represent s.d.). e) Langmuir fitting curve for GET adsorption on MNPs. Red dots represent the adsorption measured on MNPs, and black line represents the nonlinear fitting of Langmuir isotherm. Values represent mean ± s.d. (n = 4).

Table 1. Physical characterization of GET–MNPs.

	DH [nm][a)]	PDI[b)]	Zeta potential [mV]
MNPs	320.9 ± 21.6	0.16 ± 0.04	−26.2 ± 6
GET–MNPs (4 nmol mg^{-1})	310.2 ± 12.8	0.16 ± 0.03	11.7 ± 1.5
GET–MNPs (8 nmol mg^{-1})	309.4 ± 11.7	0.16 ± 0.02	20.3 ± 0.8

The size and zeta potential of the bare and GET functionalized MNPs in water (dH2O) were measured using Malvern Nanosizer Nano ZS. Values represent mean ± s.d. (n = 6 independent experiments); [a)]Z-average hydrodynamic diameter extracted by cumulant analysis of the data; [b)]Polydispersity index from cumulant analysis.

binding interactions and phenomena involved very difficult. Current models to describe protein adsorption present certain limitations, however, they can be used with caution to estimate parameters that are relevant for particle formulation.[44] A red fluorescent (TAMRA-tag grafted on an N-terminal cysteine group in P21-8R) version of GET (termed GET-T) was used to assess interaction by binding isotherms of peptide to MNPs with fluorometry. In this context, Langmuir's approximation (Equation 1) was used to fit the adsorption isotherms due to its ability to estimate relevant parameters such as maximum concentration of bound protein in a monolayer formation (S_{max}) as well as the equilibrium constant for the adsorption (K).[44–46] We plotted adsorbed

Table 2. Langmuir parameters for GET-T adsorption on MNPs.

	S_{max} [nmol mg^{-1}]	K [mL nmol^{-1}]	SSR [nmol^2 mg^{-2}]
GET–MNPs	44 ± 8.6	1.2 ± 0.2	2.0 ± 2.5

Table shows parameters of adsorption S_{max} (maximum concentration of GET that can adsorb onto 50 µg of MNPs), the constant of adsorption K, and the sum of squared residuals (SSR) corresponding to the Langmuir fitting curves displayed in Figure S4 and Table S2 in the Supporting Information. Values represent mean ± s.d. $n = 4$ independent experiments.

fraction of GET-T versus the free concentration in solution at equilibrium and nonlinear regression to adjust the experimental data (Figure 1e; Figure S4, Supporting Information). Langmuir parameters are displayed in **Table 2** (with Table S2 in the Supporting Information).

This model provides an estimate reference concentration for MNP saturation with GET peptide, which would be important for future assays (indicating MNPs are saturated by GET-T at around 40 nmol mg^{-1} MNPs after a 10 min incubation).[47,48] Similarly, the equilibrium constant of 1.2 mL nmol^{-1} demonstrates a relatively high binding efficiency of GET to the MNP, suggesting a reasonably stable NP formulation. Therefore, strong electrostatic interaction between the P21-8R GET peptide and dextran-coating of MNPs was capable of efficiently coating the MNP surface; which, except for charge, did not significantly change NP physical properties.

2.3. GET–MNPs Have Enhanced Intracellular Delivery Even with Low Amounts of Complexation

Previously, we have shown that exceptional levels of internalization and cell-loading of iron oxide can be achieved by GET conjugation.[9,27] Next, we aimed to understand the level of binding required for this enhanced uptake activity, without compromising cell viability and proliferation. We assessed the ability of GET to enhance particle uptake in mammalian cells (NIH3t3 mouse fibroblast cells) using a range of GET:MNPs ratios (**Figure 2**a). MNPs and GET–MNPs were delivered to cells overnight (16 h) and MNP-cell association (that retained with the cell pellet after harvesting) was quantitatively assessed by inductively coupled plasma mass spectroscopy (ICP-MS) (Figure 2a; Table S3, Supporting Information). GET–MNPs significantly enhanced MNP cell association from 3.2 pg Fe per cell (50 µg of MNPs alone) to 15 pg Fe per cell (50 µg of GET–MNPs). This was achieved at a GET:MNPs ratio of 4 nmol mg^{-1} MNPs, a dose that is tenfold lower than the estimated for particle saturation (44 nmol mg^{-1} MNPs). Uptake was progressively increased (in a linear fashion) with no further enhancement of interaction or uptake beyond this dose of GET (4 nmol mg^{-1} MNPs). This data demonstrates only small amounts of GET peptide complexation is required for significantly enhanced MNP cell association.

For particle characterization and subsequent delivery to cells, we used this GET peptide amount as a standardized dose above the maximum effective dose but significantly below MNP saturation (4 nmol mg^{-1} MNPs). We chose this particular formulation looking to: a) obtain reproducible delivery efficiency; and b) ensure that small changes in interaction between GET and MNPs resulted in changes in particle uptake (delivery efficiency is significantly lower at doses below 4 nmol mg^{-1} MNPs; Table S3, Supporting Information). Furthermore, we confirmed that enhanced cell uptake through GET at these dosages does not have an effect on cell viability and proliferation (Figure S5, Supporting Information).

2.4. GET Complexation with MNPs Is Stable and Does Not Promote Aggregation in Serum Conditions

We were interested in further understanding the mechanism underlying GET-mediated enhanced MNP uptake. In this context, it was important to confirm how the properties of both noncomplexed and GET–MNPs changed when exposed to the complex molecular environment of serum (in cell culture) and how that affected particle delivery. During the process of particle formulation and delivery, successive physicochemical changes on the MNPs by complexing GET peptides and further delivering in serum containing media, could potentially lead to a destabilization of the particle surface and aggregation. It has been reported that aggregation could potentially increase cell association in certain cell lines, by adsorbing onto the cell membrane providing false positives on particle delivery.[49] Other reports, however, suggest that changes in particle size and shape due to aggregation could change the uptake pathway of the particles by cells.[50,51] Therefore, understanding aggregation is key to understand whether the reported enhanced delivery (Figure 2a) is effectively mediated by GET directly or whether it could be attributed to precipitation of aggregates. Particle size distribution (measured by DLS) and zeta potential were analyzed immediately after particle complexation (day 1) and after 24 h incubation (day 2) in an attempt to mimic the behavior of particles over the delivery process in vitro (Figure 2b,c). MNPs and GET–MNPs in serum (the in vitro delivery conditions for cells) showed similar zeta potential distribution profiles with an average zeta potential of around −6 mV (Table S7, Supporting Information), suggesting the interaction of both particles (MNP and GET–MNP) with negatively charged proteins in serum. There are no significant differences in particle size between MNPs and GET–MNPs (271.8 ± 9.64 nm and 276.7 ± 8.58 nm, respectively; Table S4, Supporting Information). We carefully assessed the area under the curve (AUC) of the size distribution of i) main peak and ii) aggregate peak of MNPs and GET–MNPs (Figure 2c-i; Figure S5, Supporting Information). Aggregates account for 2–5% of the total size distribution area, and there were no significant differences between aggregate formation in MNPs and GET–MNPs (Figure 2c-ii). Furthermore, there were no significant differences in the size distribution of the main peak of immediately complexed samples, or those at day 1 and day 2 postcomplexation (Figure 2c-i; Figure S6, Supporting Information). In summary, we found no differences in particle size or distribution for MNPs and GET–MNPs after prolonged incubation in cell culture conditions. Therefore, our analyses suggest

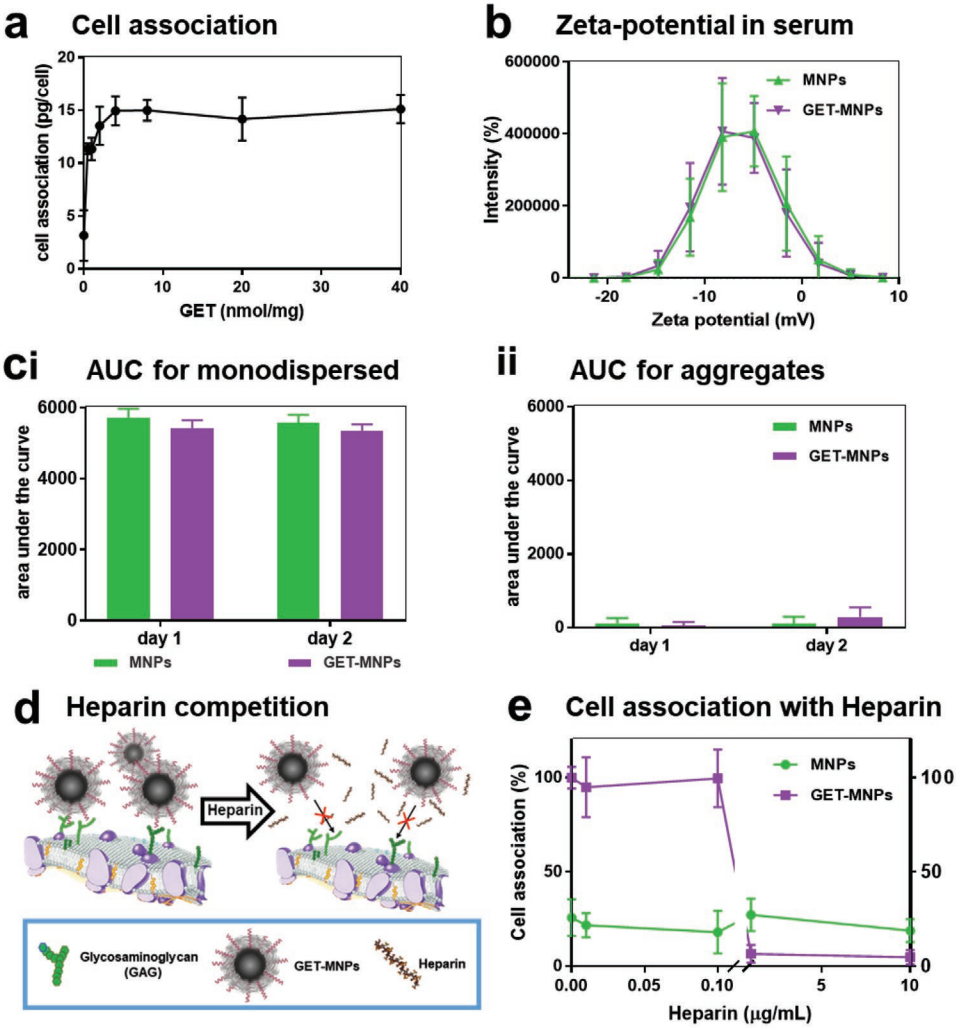

Figure 2. Enhanced MNPs uptake is mediated by cell surface GAG. a) Iron cell association in NIH3t3s in the presence of MNP (50 μg) and increasing concentrations of GET (0.5, 1, 2, 4, 8, 20, and 40 nmol of GET mg^{-1}). Iron cell association was measured by ICP-MS. Values represent mean iron association per cell ± s.d. ($n = 6$). b) Zeta potential of particles 50 μg incubated with 4 nmol mg^{-1} GET. Zeta potential was measured in 10% FCS. MNPs and GET–MNPs present similar charge distribution ($n = 6$ independent repeats, 3 subruns per repeat). c) Area under the curve (AUC) for the size distribution of MNPs and GET–MNPs of the i) main peak and ii) aggregates. Values represent mean area under the curve ± s.d. ($n = 6$). d) Schematic representation of hypothesized mechanism for heparin interference in GET–MNPs interaction with the cells. e) Percentage of cell association in NIH3t3s of GET–MNPs at increasing concentrations of heparin (0, 0.01, 0.1, 1, and 10 μg mL^{-1} heparin). Percentage of cell association was calculated taking cell association in the absence of heparin as 100%. Values represent mean iron association per cell ± s.d. ($n = 6$).

that GET-mediated enhanced particle uptake was not significantly driven by progressive changes in particle charge, size, or aggregation.

2.5. GET–MNP Uptake and Not Complexation Is Directly Influenced by Heparin

Our proposed uptake mechanism for the GET system is based on the interaction of GET peptides with GAGs present on the cell membrane; this interaction in the presence of a CPP triggering the start of uptake by endocytotic processes (Figure 2d).[27] We assessed MNP delivery at increasing concentrations of heparin, which has been shown to serve as a competitive inhibitor of cell uptake by GET.[27] Heparin is a soluble highly sulfated and specific form of heparan sulfate generated by mast cells and has been previously used as a GAG competitor.[52] Heparin inhibits GET-mediated cell association by 93% (from 99.6% of particle uptake at 0.1 μg mL^{-1} heparin to 6.5% of particle uptake at 1 μg mL^{-1} heparin) (Figure 2e). Noncoated MNP uptake remains unaffected by even the highest concentration of heparin. Prussian Blue staining confirms the same trend and demonstrated uniformity across all cells tested (Figure S7, Supporting Information). It was unclear as to whether heparin-mediated inhibition was mediated by competing and removing the GET peptide:MNP electrostatic coating. This was important to determine as it could be argued that the decrease in cell association could be due to heparin destabilizing GET:MNPs interaction, causing peptide detachment from the MNPs and hence minimizing cell uptake

indirectly. In order to test this, red fluorescently tagged GET (GET-T) was adsorbed onto MNPs and then incubated with increasing concentrations of heparin (Figure S8, Supporting Information); assessing the amounts released from the MNP by fluorometry. The data demonstrates that heparin does not have a significant effect on the amount of GET desorbed from MNPs compared to control (phosphate-buffered saline; PBS) even up to concentrations as high as 100 μg mL^{-1}, which prevented any enhancement of uptake by GET coating in the cell assays. Taken together, these results suggest that heparin inhibits GET-enhanced uptake of MNPs at the level of the cell membrane interaction and that the presence of GAGs in the cell surface is likely required for the enhanced particle association mediated by GET. This agrees with our more rigorous analyses in the studies that originally described GET delivery.[27]

2.6. GET Mediated Enhanced MNP Cell Association Is Rapid and Not Dependent on Cell-Type

We showed GET-mediated enhanced NP-cell association at low peptide concentrations. Next, we aimed to demonstrate that GET enhanced NP delivery was not cell type dependent. GET–MNPs (4 nmol mg^{-1} MNPs) were delivered to NIH3t3s (fibroblasts), U87 (glioma), and hMSCs (mesenchymal stem cells). All cell types showed at least threefold increase on particle association in the presence of GET (**Figure 3**a). Prussian Blue staining confirmed the presence of intracellular iron in hMSCs (Figure 3b). MNP delivery was also performed in serum free conditions confirming similar uptake profiles as that seen in protein-rich conditions (Figure S9, Supporting Information). Interestingly, the cell types behaved differently in the presence of serum; however, GET–MNPs had significantly enhanced cell association independent of cell type and media used.

2.7. GET Mediated MNP Cell Membrane Association Leads to Enhanced Uptake

To confirm that cell association indeed represented intracellular delivery and not simply extracellular membrane-associated MNPs, we performed microscopic analyses of embedded cell suspensions to assess MNP localization. Dual beam (focused ion beam-scanning electron microscopy; FIB-SEM) images of individual BV2 cells (immortalized murine microglial cell line) showed localization of internalized MNP aggregates in large clusters (≈500–1000 nm) around the cell nucleus confirming perinuclear accumulation of MNPs in endosomal vesicles (Figure 3c). Similarly, TEM images of NIH3t3s after 24 h delivery of MNPs (Figure S10, Supporting Information) show accumulation in intracellular vesicular structures that resemble endosomes.

2.8. Extracellular Membrane Associated GET–MNPs Are Rapidly Internalized

Understanding the kinetics of MNP uptake was considered essential to further characterize GET mediated enhanced delivery. Iron content of the delivery media (including washes and trypsin; termed non-cell associated) and iron content within cells (after washing and trypsinization, representing just the cell pellet; termed cell associated) were analyzed at 0.5, 2, 4, 6, and 24 h postdelivery of MNPs and GET–MNPs (Figure 3d). MNP uptake in cells is a process determined by factors such as flux across the cell membrane, endosome dynamics, and vesicular transport toward lysosomes. At early time points these processes are mainly considered to be concentration dependent and intracellular concentration of MNPs should appear to increase almost linearly. However, at later time-points, energy depletion and decrease in the number of endocytosis domains from the cell surface account for linearity deviation and eventually reach a steady state of uptake concentration.[53] This is the case for all our uptake experiments where for the first 4 h the concentration of iron associated with cells increased linearly with time, this independent of initial particle concentration or particle type (MNP or GET–MNPs) (Figure 3d). Linear approximation was calculated using the iron uptake interval between 0.5 and 4 h as it had been previously reported (Figure S11, Supporting Information).[54] There are significant differences in the slope of the curves (kinetic constant), which were proportional to the dose and significantly higher for GET–MNP (Table S6, Supporting Information). After 4 h, the concentration of iron in the cells against time starts to deviate from linearity (with larger deviations for the higher particle doses) toward a logarithmic fit, where the concentration of MNPs per cell remains almost constant up to 24 h. This kinetic model suggests that the final concentration of iron in the cells is mostly determined by the cellular uptake that takes place within the first 4 h. Significantly different kinetic constants of GET mediated delivery suggest that uncoated MNP uptake is not mediated by the same receptors (Table S6, Supporting Information). Our kinetic analyses similarly confirms significant differences in final concentrations of iron cell association for MNPs and GET–MNPs as strong evidence for this. Physicochemical properties and concentrations were the same for both experiments, almost identical sizes and charges in the presence of serum, so that only different cell surface binding/receptors and uptake mechanisms would account for different final uptake concentrations.[54,55] As expected the iron concentration in extracellular media decreases overtime inversely proportionally to the uptake of iron by cells providing an important technical control (Figure S12, Supporting Information).

2.9. Intracellular GET–MNPs Are Not Significantly Exported or Rapidly Degraded

Iron recycling, being iron secreted extracellularly from cells after uptake, was analyzed up to 4 days postdelivery. Our data showed no significant differences in the pattern of iron recycling of cells incubated with MNPs or GET–MNPs, and the percentage exported was in all cases below 5% over the 3 days assessed postdelivery (Figure S13, Supporting Information). These results were consistent with the literature, and add to the argument that GET–MNPs are internalized and are not exocytosed or degraded rapidly inside of cells.[56]

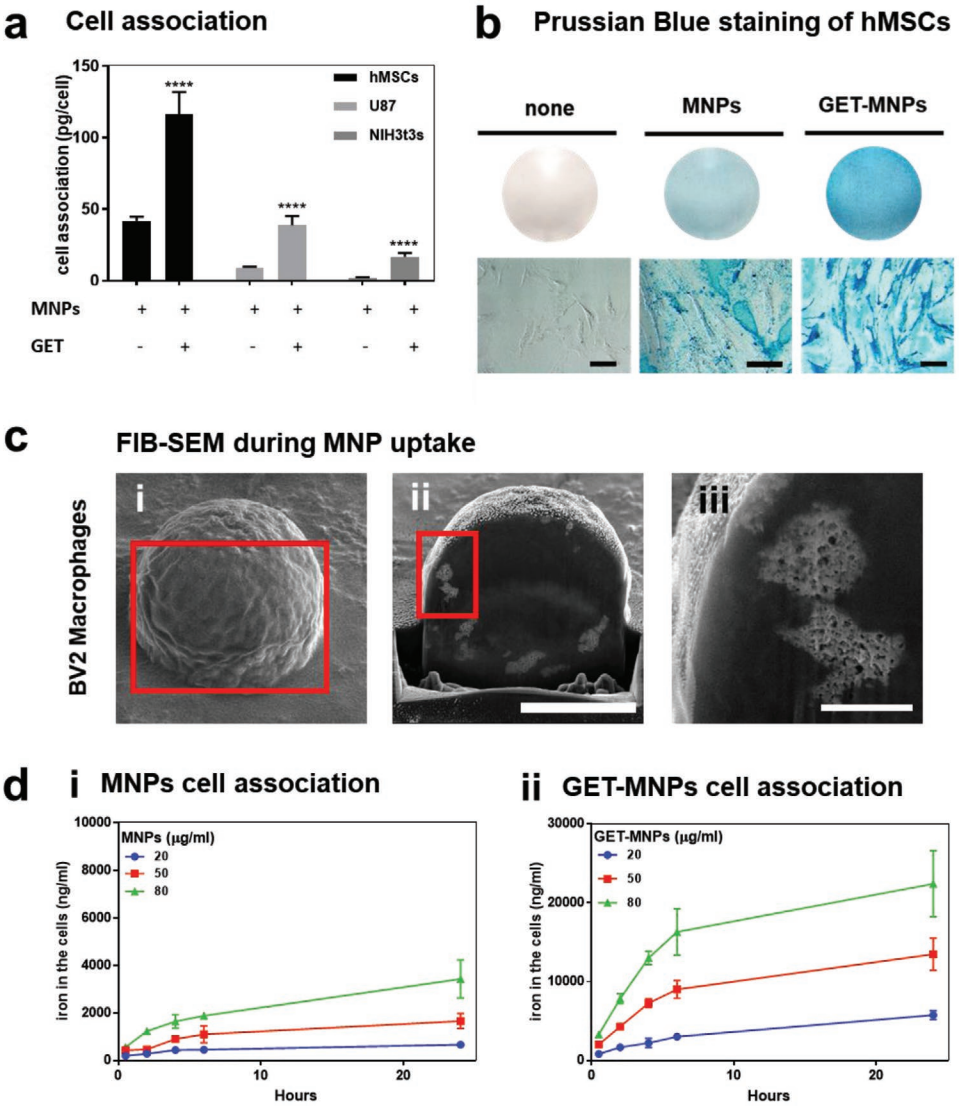

Figure 3. GET–MNPs have enhanced cell uptake in vitro. a) Iron cell association after delivery of 50 µg MNPs or GET–MNPs. Particles were delivered to: human mesenchymal stem cells (hMSCs), human glioblastoma cells (U87), and mouse embryonic fibroblasts (NIH3t3s). Iron cell association was measured by ICP-MS. Values represent mean iron association per cell ± s.d. ($n = 6$, $^{****}p < 0.0001$ Sidak's multiple comparisons test, compared to MNPs alone). b) Representative light microscopy images of Prussian Blue iron-stained hMSCs treated with 50 µg MNPs or 50 µg MNPs–GET for 12 h. When MNPs are delivered without GET, the iron staining is localized mainly around the cells. MNPs are taken into hMSCs most efficiently when delivered with GET (GET–MNPs). Circular image of entire well (scale bar: 50 µm). c) FIB-SEM images of individual BV2 microglial cells show the presence of dense agglomerates of MNPs inside the cell. BV2s were treated with 500 µg GET–MNPs (estimated 50 pg Fe per cell). Scale bars: i) 5 µm; ii) 4 µm; iii) 500 nm. d) Iron cell association for i) naked MNPs delivery and ii) GET–MNPs over time in NIH3t3s at increasing dosages of MNPs (20, 50, and 80 µg). Iron content in the cells was measured 0.5, 1, 2, 4, 6, and 24 h postdelivery using ICP-MS. Values represent mean percentage of iron cell association ± s.d. ($n = 6$).

2.10. GET Enhanced MNP Delivery Is Not Affected by Serum or Plasma Protein Corona

After characterizing the mechanism of enhanced MNP uptake mediated by GET peptide complexation, we wanted to further assess the effect of extracellular microenvironmental conditions on the interaction of MNPs with cell membranes and their subsequent intracellular uptake. Importantly, all in vitro experiments presented so far had been performed in the presence of serum proteins (growth media containing 10% fetal calf serum; FCS, termed GM). It has been reported that targeting systems can lose uptake efficiency, and can be even negated when employed in the presence of serum compared to delivery in serum-free media (**Figure 4**a).[19,57,58] Plasma is the fluid component of blood devoid of cells and platelets but has high concentrations of fibrinogen and other clotting agents, while serum is clotted plasma depleted of these components.[59] Interestingly some studies use serum and plasma addition interchangeably when testing the effect of biological milieu on NPs, however, recent research has shown significant

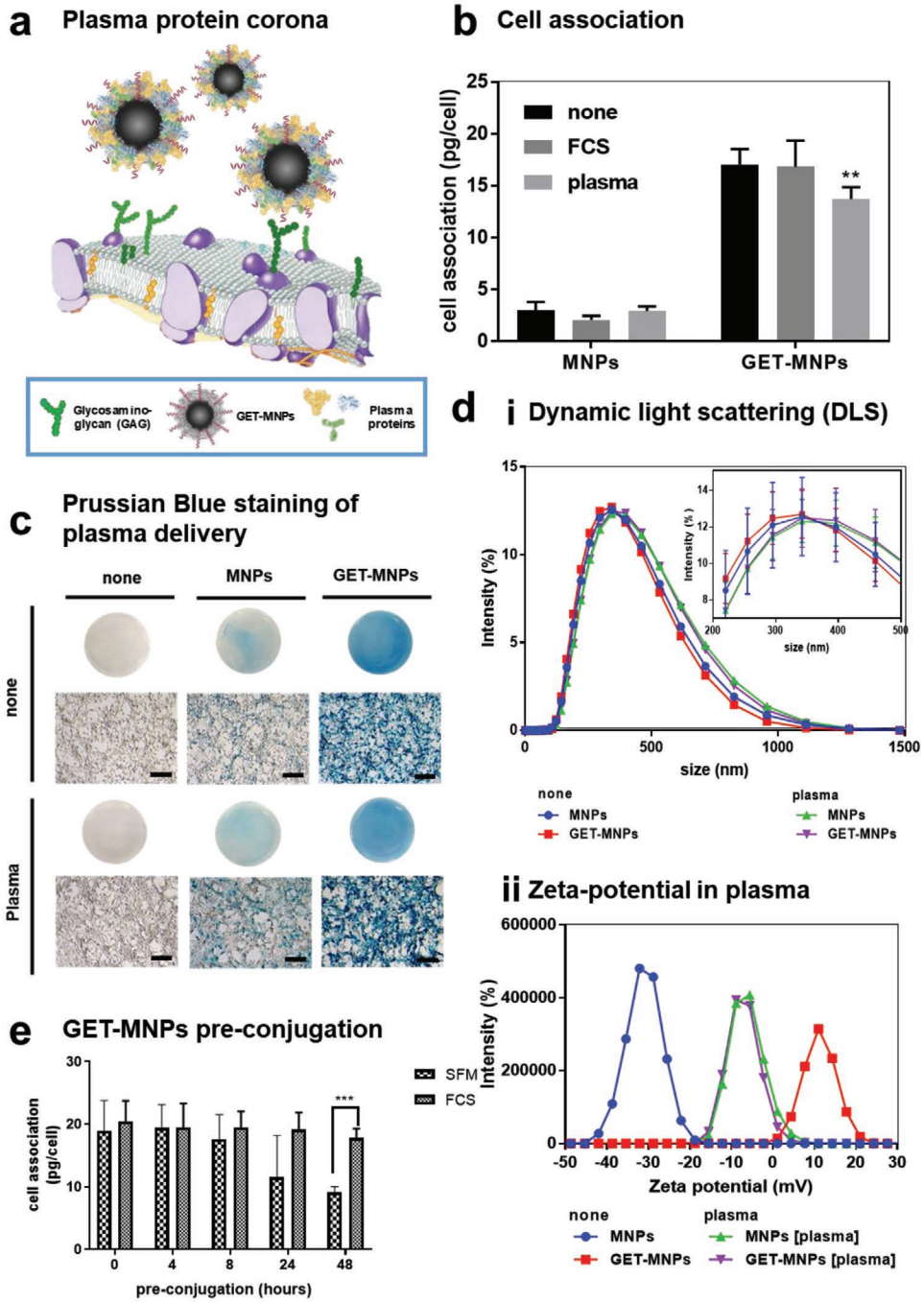

Figure 4. GET–MNPs have enhanced uptake in vitro in the presence of plasma. a) Schematic of hypothesized GET–MNPs interaction in the presence of plasma proteins. b) Iron cell association after overnight delivery of MNP and GET–MNPs in serum free media (none), 10% FCS v/v in water (FCS), and 5% plasma v/v in water (plasma). Iron content was measured by ICP-MS. Values represent mean iron cell association per cell ± s.d. ($n = 6$, $^{**}p < 0.01$ Tukey's multiple comparisons test, compared to FCS). c) Representative light microscopy images of Prussian Blue iron-stained NIH3t3s treated with 50 µg MNPs or 50 µg MNPs–GET (4 nmol mg^{-1}) for 12 h in serum free media (none) and at 5% plasma (plasma) (circular image is of entire well). Scale bar: 50 µm. d) Physicochemical characterization of GET–MNP in the presence of plasma proteins. i) The apparent diameter of MNPs and GET–MNPs in water is shown for reference ($n = 6$ independent repeats, 3 subruns per repeat, error bars in the close-up plot represent s.d.). ii) Zeta potential distribution of MNPs and GET–MNPs in 5% plasma v/v in water. The zeta potential of MNPs and GET–MNPs in water is shown for reference ($n = 6$ independent repeats, 3 subruns per repeat). e) Iron cell association after delivery of preconjugated GET–MNPs. GET–MNPs were formulated and incubated for 0 (control), 4, 8, 24, and 48 h in SFM or GM containing 10% FCS v/v (FCS). Iron content in the cell was measured 24 h postdelivery by ICP-MS. Values represent mean iron association per cell ± s.d. ($n = 6$, $^{***}p < 0.001$, Sidak's multiple comparison test).

differences between plasma and serum in terms of protein corona composition.[60,61]

It was therefore important to assess the differences in particle size and cellular uptake between the two milieus: plasma (unclotted containing fibrinogen and other factors) versus serum (clotted and lacking fibrinogen). Initially, unlike for serum or serum albumin, we found it technically difficult to coat and purify MNPs away from plasma without obtaining a significant degree of aggregation either using centrifugation or a static magnet (data not shown), which made delivery very variable and difficult to reproduce. Furthermore, delivery and characterization assessments were precluded in 100% plasma, as we found pure plasma significantly affected cell viability in cultured lines, inhibiting the reproducibility of the delivery data.

MNPs and GET–MNPs were delivered in serum-free media (SFM, no protein), 5% plasma (see "MNP delivery in plasma" in the Experimental Section and Figure S14 and Table S7 in the Supporting Information) and 10% FCS (GM) incubation experiments with NIH3t3 cells (Figure 4b,c). GET peptide complexation significantly and consistently enhanced MNP uptake regardless of media protein content. Delivery of GET–MNPs in plasma conditions was minimally but significantly lower than in serum free or serum-containing media. This could be attributed to the effect of plasma on cells directly but minimally affecting uptake.

2.11. Plasma Coronas Only Generate Subtle Changes in GET–MNP Physicochemical Properties

So far, significant emphasis was placed on the full characterization of the GET–MNP interaction prior to delivery experiments but very little characterization had been undertaken within a cell culture or in vivo microenvironment. The composition of most biological media (containing serum or plasma proteins and different ions) has the potential to alter MNP surface properties. For instance, dissolved ions may neutralize charged chemical groups on the particle surface and favor an exchange process between molecules in solution and the surface associated molecules.[62] To confirm the physicochemical properties in more biologically relevant conditions, we assessed particle size, charge, and size distribution in plasma. Both MNPs and GET–MNPs retained stability, with minimal changes in particle size or size distribution with incubation in 5% plasma compared to water (Figure 4d-i; Figure S15 and Tables S8–S10, Supporting Information). Interestingly, there were small but significant differences in size between uncoated MNPs incubated in plasma and serum, suggesting a difference in the protein corona formed. Size differences were not observed for GET–MNPs (Table S8, Supporting Information). Similarly, to what was previously observed in serum, the presence of plasma proteins and ions significantly affected the particle charge, giving both MNPs and GET–MNPs identical negative charges (around −10 mV) (Figure 4d-ii). These findings have been described in literature suggesting that the formation of serum or plasma protein coronae leads to a normalization of the particle zeta potential.[63] When assessing aggregate formation over longer incubation periods in the presence of plasma (Figure S15e,f, Supporting Information), we observed a significant increase in MNPs aggregation and some loss of colloidal stability on day 2, however there were no significant differences in aggregation between MNPs and GET–MNPs that could account for the differences in cell uptake observed. Finally, seeking to further confirm the stability of the particles in serum, we preconjugated GET–MNPs and incubated them for up to 2 days (48 h) in SFM or GM. GET–MNPs were then delivered to cells overnight and cell association was quantified by ICP-MS (Figure 4e; Table S9, Supporting Information). Interestingly, GET–MNPs retained their full delivery efficiency for up to 48 h only when they were incubated in GM.

These results suggest that regardless of differential interaction of plasma proteins with MNPs and GET–MNPs, the activity of GET peptide is significantly retained on MNPs and still promotes enhanced intracellular particle uptake. Additionally, serum proteins maintained GET–MNPs enhanced uptake over time, suggesting that protein coronae could play a role in stabilizing GET–MNPs in vitro.[64] Importantly, this data also confirms that positive charge is not absolutely required for the enhanced endocytosis mediated by GET to occur.[27]

2.12. Rapid, Specific, and Evolving Protein Corona Formation on GET–MNPs

In order to qualitatively confirm the formation of plasma protein coronas on MNPs and GET–MNPs, we exposed them to pure human plasma for 10 min, rapidly removed and washed away excess unbound protein by centrifugation, and ran samples directly on sodium dodecyl sulfate-polyacrylamide gel electrophoresis (SDS-PAGE) gels. Denaturing electrophoresis revealed similar protein composition of the protein corona formed on MNPs and GET–MNPs; however, there were subtle differences in presence of some bands and band intensity when compared to whole plasma protein species (**Figure 5**a).

To gain a deeper insight of the effect of GET on the protein corona formation on MNPs, we used label-free snap-shot proteomics using liquid chromatography mass spectroscopy (LC-MS). The composition of the protein corona was assessed at two different time points to determine whether exposure time (acute, 1 min; chronic, 30 min) had an effect on the protein profile. There were no differences in the number of proteins identified between the two exposure times (167 proteins). This agrees with previously published research which reported that out of the thousands of proteins present in plasma only a few tens of proteins bind to NPs at significant quantities (>1 molecule per single MNP).[24,65]

Further analysis showed that negatively charged proteins at physiological pH (isoelectric point between 5 and 7) represent the majority of the corona components for both MNPs and GET–MNPs, irrespective of the particle initial surface charge or exposure time (Figure 5b-i). This finding is in accordance with the previously reported zeta potential results that show that NPs exposed to plasma present an overall negative charge irrespective of their original charge (Figure 4d; Table S8, Supporting Information). These results once again reinforce the hypothesis that the overall charge of NPs is not a driving factor in the uptake process, and suggest that despite protein corona formation, GET is still available and able to interact with the

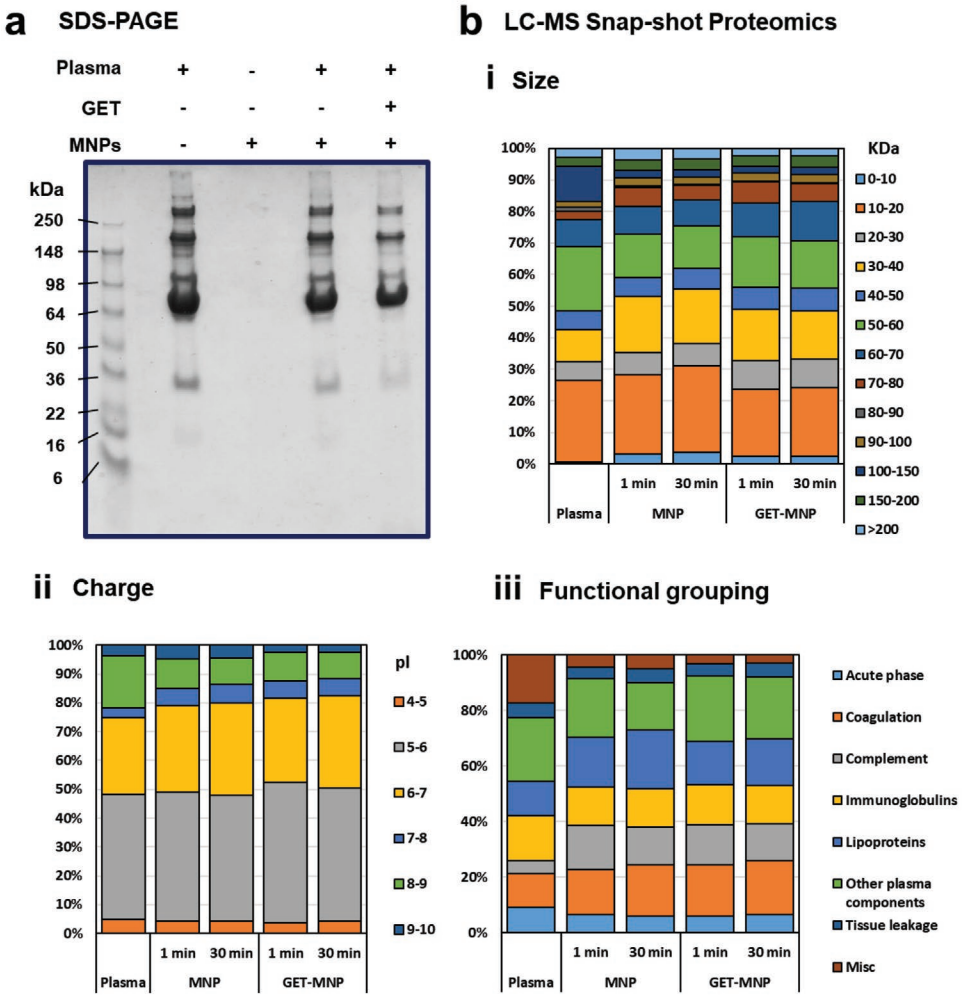

Figure 5. Specific GET–MNP protein corona formation by SDS-PAGE and LC-MS. a) Separation of plasma proteins adsorbed on MNPs and GET–MNPs after 30 min incubation on 12% SDS-PAGE gel. Molecular mass and sample characteristics are indicated. b) Classification of corona proteins identified by LC-MS on MNPs and GET–MNPs after 1 and 30 min exposure to plasma. Proteins were classified according to i) calculated molecular weight, ii) isoelectric point, and iii) functional grouping. Relative percentages of protein abundance are shown ($n = 2$, independent experiments).

cell surface mediating endocytosis.[25,63,64,66] Evolution of proteins over time follows similar patterns in MNPs and GET–MNPs (Figure 5b) indicating a strong interaction of plasma proteins with the dextran on the particle surface.[67] This suggests that for the most part, the kinetics of those interactions are not affected by the presence of GET peptide.

We examined the most abundant proteins forming coronae on MNPs and found differences among the top 15 most abundant proteins forming MNPs and GET–MNPs coronas after 1 and 30 min incubation; this was significantly different to analyses of plasma alone (**Table 3**; Tables S11 and S12, Supporting Information). Data indicated an enrichment of certain plasma proteins within the MNP protein corona. Prothrombin is seen to be more commonly abundant in GET–MNPs than in MNPs (after 1 and 30 min of exposure). We compared the relative abundance of the proteins present in the protein corona of MNPs and GET–MNPs in order to identify proteins that were differentially present in the protein coronae (Figures S17 and S18, Supporting Information). We found that prothrombin (accession number: P00734) and vitamin K-dependent protein S (accession number: P07225) were significantly more abundant in GET–MNPs after 1 min exposure. After 30 min incubation, immunoglobulin heavy constant gamma (accession number: A0A087WV47) and prothrombin were significantly more abundant in the protein corona of GET–MNPs compared to MNPs. We were not able to identify any proteins that were significantly enriched in the protein corona of MNPs alone. The consistent enrichment of glycoproteins in GET–MNPs indicates the formation over time of a specific corona tailored by the GAG-binding domain in GET peptide.

Interestingly, the protein corona evolution over time could corroborate previous findings suggesting that protein coronae are formed of two layers. The first layer (most internal) is hypothesized to be formed of biomolecules that are more tightly bound to the particle (termed hard corona), and an outer layer that interacts more loosely with the particle surface and interacts more readily with the environment (termed soft corona)[65] which are the most evolving constituents.

Table 3. Top 15 most abundant corona proteins (NSAF) after 1 min of plasma exposure.

	MNPs	GET–MNPs
1	Apolipoprotein A-I	Apolipoprotein A-I
2	Serum albumin	Serum albumin
3	Fibrinogen gamma chain	Prothrombin[a)]
4	Apolipoprotein C-III	Ig kappa chain C region
5	Fibrinogen beta chain	Fibrinogen gamma chain
6	Apolipoprotein C-I (fragment)	Fibrinogen beta chain
7	Ig kappa chain C region	Apolipoprotein C-III
8	Apolipoprotein A-II	Serotransferrin
9	Serotransferrin	Apolipoprotein A-II
10	Apolipoprotein E	Apolipoprotein C-I (fragment)
11	Fibrinogen alpha chain	Transthyretin
12	Transthyretin	Fibrinogen alpha chain
13	Apolipoprotein A-IV	Apolipoprotein E
14	Kininogen-1	Apolipoprotein A-IV
15	Ig lambda-2 chain C regions (fragment)	Vitamin K-dependent protein Z[a)]

The majority of proteins identified are common for MNPs and GET–MNPs; [a)]Most abundant proteins in GET–MNPs that are not present in MNPs are glycoproteins. $n = 2$ independent experiments.

Even though proteomic analyses demonstrated only minimal differences in the protein coronae formed, it is important to remember that specific plasma proteins have dedicated cell surface receptors in order to mediate their biological functions. The successful enhancement of MNP uptake in the presence of GET peptide complexation indicates that the affinity of GET peptides for GAGs presented on the cell membrane is greater to or compatible with other interactions elicited by the plasma molecules that form its protein corona.[25]

2.13. GET–MNP Corona Prevents Hemotoxicity and Aggregation

The biological effects of the plasma protein corona on GET–MNPs were demonstrated on human erythrocytes (red blood cells; RBCs) since they are present in high concentrations in blood and are likely to be one of the first cell-types that interact with NPs as they enter the blood system in several biotherapeutic applications.[68]

Human erythrocyte aggregation and cell morphology were assessed after exposure to GET–MNPs for 5, 15, 30, and 60 min in saline (PBS) or human plasma. Cells were also incubated with MNPs or GET peptide alone, and compared to Lipofectamine 2000 (commercial transfection agent, Life Technologies). Time-course experiments assessing aggregation of erythrocytes were conducted in both PBS and plasma (Figures S19 and S20, Supporting Information, respectively). No significant changes in cell morphology were observed with MNPs or GET–MNPs (Figures S19 and S20, Supporting Information). Cell morphology was immediately (<5 min) affected after incubation with Lipofectamine 2000 in PBS (Figure S19, Supporting Information). Interestingly, GET peptide alone in high concentration progressively induced cell morphological changes over time in PBS (**Figure 6**a; Figure S19, Supporting Information). GET peptide-induced cell morphology could potentially be mediated by the interaction of the peptide with glycoproteins present in the erythrocyte cell membrane.[69] However, these changes in morphology were not observed when GET was adsorbed onto the MNPs (GET–MNPs) or in the presence of plasma. Additionally, the difference in osmolarity between the plasma and PBS could account for some of these morphological changes in erythrocytes.[70]

No significant effects in aggregation or cell morphology were observed in human plasma except for Lipofectamine 2000, which progressively induced cell aggregation in the form of stacks, this phenomenon known as Rouleaux aggregation[71] (Figure S20, Supporting Information). This is associated with the presence of fibrinogen; however, other macromolecules such as dextran have also been reported to induce this phenomenon. Rouleaux aggregation is reversible, but in certain cases, it can lead to erythrocyte sedimentation and can be an indicator of disease.[71] The mechanism underlying this aggregation process is still not well understood, however, macromolecules in solution seem to play a role as bridging agents between adjacent erythrocytes.

We further investigated the effect of the GET peptides and MNPs in erythrocyte cell lysis (hemolysis). The percentage of erythrocyte lysis was calculated compared to the effect of Triton-X 100 (1% v/v), which permeabilizes and ruptures erythrocyte cell membranes (Figure 6b; Figure S21, Supporting Information). Lipofectamine 2000 was analyzed as a control commercially available transfection reagent. After 30 min, MNPs, GET, and GET–MNPs have similar low effect on hemolysis in PBS. Rapid corona formation in plasma efficiently prevented hemolysis for MNP and GET–MNP incubated erythrocytes (Figure 6b). Our data therefore demonstrates that soluble GET or GET–MNPs do not create aggregation or lysis of erythrocytes in the presence of the endogenous blood protein complexity provided by serum or plasma.

3. Conclusions

Our study demonstrates that GET peptide functionalized MNPs are capable of significantly enhancing MNP cell uptake in serum and plasma conditions (by up to eightfold). This increase in uptake was not due to aggregate formation and was mediated by GET-heparan sulfate interactions. Furthermore, in a physiologically relevant environment, highly complex protein coronas are rapidly formed on GET–MNPs. These coronae evolve but do not dramatically change over time. In addition to this, we found that even if most corona proteins coating MNPs and GET–MNPs are the same, there are subtle differences in the relative abundance of the proteins present, as well as a small number of specific proteins on GET–MNPs. This suggests that GET peptides can direct some plasma protein binding and subtly change the protein coronae formed.

We are aware that this study has some limitations and future more in depth analysis of the MNP protein corona

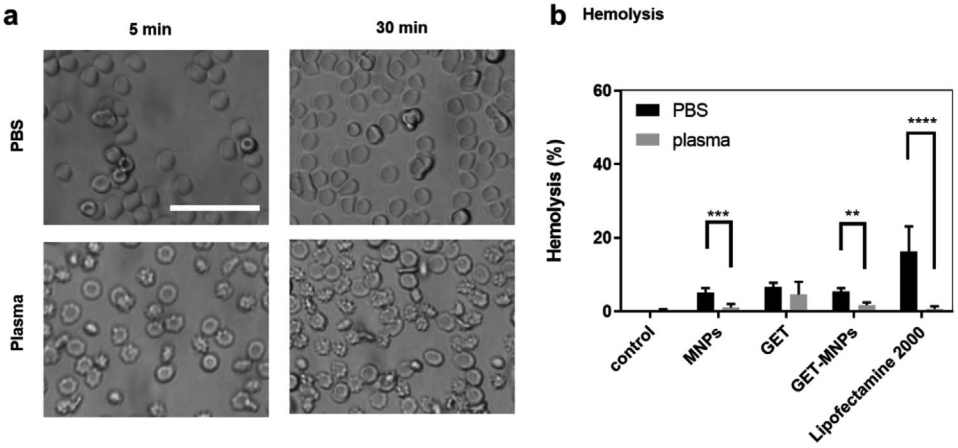

Figure 6. GET exposure does not trigger erythrocyte hemolysis. a) The effect of GET (0.4 nmol mL^{-1}) on erythrocytes after 5 and 30 min in PBS and plasma. Scale bar: 20 µm. Close-up images were taken from Figures S19 and S20 in the Supporting Information. b) Hemolysis of erythrocytes. Erythrocytes were exposed to 100 µg mL^{-1} MNPs (MNPs), 0.4 nmol mL^{-1} (GET), and 100 µg mL^{-1} GET-MNPs (4 nmol mg^{-1}) in PBS or plasma for 30 min. They were also treated with Triton-x 100 (positive control for lysis) and Lipofectamine 2000 as comparison for transfection reagent. Values represent mean ± s.d. from 4 independent repeats from the same donor. Hemolysis was significantly affected by rapid protein corona formation in particles ($n = 4$, $^{**}p < 0.01$, $^{***}p < 0.001$, $^{****}p < 0.0001$, Sidak's multiple comparison test).

development over time may be needed in order to better predict the behavior of the particles in vivo. Understanding how heparan sulfates can affect corona formation and retention will help understanding of the mechanism through which GET–MNPs can still significantly interact with cell membranes and internalize. Another important factor to be assessed is the long-term stability of GET–MNPs in the presence of plasma, and the effect of plasma salts in the interactions between GET and MNPs. Further work should also consider whether the effect of plasma on preventing erythrocyte lysis is due to the presence of extra protein bulk in media, or whether plasma proteins play a specific role in erythrocyte protection. In addition, the effect of GET peptides and coated MNPs should be assessed with other blood components (such as thrombocytes) and directly delivered in vivo.

Our study is significant, since there appears to be a division in the literature on the effect of protein coronae on functionality and specificity of cell targeting molecules in biologically relevant environments. Here our findings confirm that the presence of protein corona on GET–MNPs does not significantly affect the enhancement of particle uptake. This demonstration represents a stepping-stone to further develop GET–MNPs into a platform technology for future drug delivery applications in nanomedicine. Finally, this study provides us with a better understanding of how protein corona can affect biological function.

4. Experimental Section

Physicochemical Analysis: Nanomag-D MNPs (Fe_3O_4 core; 250 nm; product code 09-02-252) were purchased from Micromod (Germany). The size and zeta potential of the bare and GET functionalized magnetic nanoparticles were measured in water (distilled H_2O) using Malvern Nanosizer Nano ZS. Values represent mean ± standard deviation (s.d.).

DLS: Measurements consisted of 3 repeats (12–15 subruns per repeat) of the same sample to estimate the error in the measurements. The measurements were recorded at room temperature. *N* refers to the number of repeats. To measure the aggregation behavior of MNPs, particle size was measured on day 1 (particle formation and delivery) and day 2 (end of particle delivery) looking to most accurately reproduce particle delivery to cells in vitro. Main peak area was calculated between 0 and 1600 nm. Aggregate area was calculated between 3000 and 7000 nm. AUC was calculated by GraphPad Prism v 7.03.

Zeta Potential: Measurements consisted of 3 repeats (12–15 subruns per repeat) of the same sample to estimate the error in the measurements. The measurements were recorded at room temperature. Because zeta potential measurements were performed in an aqueous solution, the Smoluchowski approximation was used to calculate the zeta potentials from the measured electrophoretic motilities. *N* refers to the number of repeats. Sidak's multiple comparisons test was used to determine significant differences between samples.

TGA: The amount of dextran polymer on the particle surface was determined by TGA (TA Instruments Q 6000 STD) in a nitrogen atmosphere. MNPs were dried overnight at 80 °C before TGA measurements. 2–4 mg of particles were deposited into a platinum TGA pan. The sample was allowed to equilibrate inside the TGA furnace at room temperature, and then was ramped to 200 °C at a rate of 15 °C min^{-1}. The sample was held at 200 °C min^{-1} for 5 min, before ramping up to 600 °C at 15 °C min^{-1}. Sample was held at 600 °C for 5 min before cool-down. The organic content of the sample was estimated as the mass loss occurring between 200 and 500 °C. The fraction of mass that evaporates before 200 °C is typically assumed to be low-boiling volatiles (such as solvents, adsorbed moisture, etc.) while the fact that sample mass begins to plateau around 500 °C is taken to indicate that the organic has combusted and only the inorganic core of particles is left behind. The fraction of organic phase was calculated as the ratio between mass lost between 200 and 500 °C over the total mass at 200 °C.

Protein Adsorption—GET Adsorption: GET peptide (P21-8R) was labeled with fluorescent variant of rhodamine, 5-carboxytetramethylrhodamine (5-TAMRA, Sigma, C2734), GET-T. The following solutions of GET-T were prepared in PBS: 0.025×10^{-9}, 0.05×10^{-9}, 0.1×10^{-9}, 0.2×10^{-9}, 0.4×10^{-9}, 1×10^{-9}, and 2×10^{-9} M. GET-T. Solutions were incubated with 50 µg mL^{-1} of Micromod dextran-coated MNPs under constant agitation for 10 min at RT (this incubation time was chosen based on experimental

in vitro delivery). MNPs were magnetically separated and supernatant was collected. PBS solution was used as a control. Protein concentration was measured using a plate reader excitation 546 nm, emission 579 nm (Infinite 200 PRO, TECAN). $N = 4$, independent repeats. Standard curves were prepared for the tagged protein by plotting increasing concentrations of GET-T versus fluorescence.

Protein Adsorption—Serum Albumin Adsorption: Solutions of FITC-labeled bovine serum albumin (BSA) (Thermo Fisher, A23015) were prepared in PBS: 6.25, 12.5, 25, 50, 100, 150, and 200 μg mL^{-1}. Solutions were incubated with 50 μg mL^{-1} of Micromod dextran-coated MNPs under constant agitation for 10 min at RT. MNPs were magnetically separated and supernatant was collected. PBS solution was used as a control. Protein concentration was measured using a plate reader excitation 488 nm, emission 532 nm (Infinite 200 PRO, TECAN). $N = 6$, independent repeats.

For GET peptides and BSA, standard curves were prepared for the tagged protein by plotting increasing concentrations versus fluorescence. Background fluorescence was subtracted both from the media (PBS) and MNPs only to account for particle background fluorescence. Isotherms were adjusted using nonlinear least-squares fitting on Excel[72]

$$S = \frac{S_{\max} K C_f}{1 + K C_f} \quad (1)$$

where C_f is the solute concentration remaining in solution at equilibrium, S represents the adsorbed amount of solute at equilibrium, $S_{\max}$ is the maximum concentration of bound solute onto the MNPs, and K is the Langmuir's equilibrium constant that describes the strength of interaction between solute and the particles surface.[44]

Briefly, a function was defined in Excel to minimize the value of the sum of squared residuals (SSR). In this context, a residual was defined as the difference between the observed data and the experimental data calculated using the Langmuir equation. $S_{\max}$ and K were adjusted to obtain a minimum value for SSR.

Protein Adsorption—Conformational Assessment of Surface-Bound Proteins: Infrared analysis of surface-bound GET was conducted using a Thermo Fisher Scientific Nicolet iS50 FT-IR Spectrometer. Spectra were recorded at 4 cm^{-1} resolution with 36 scans being averaged, smoothed by 9 point adjacent averaging and curve fitted. OMNIC software was used to identify and analyze the spectra. Briefly, adsorption band regions in the amide 1 band were estimated from the wide range of literature: alpha helix (1646–1656 cm^{-1}), beta sheets (1628–1640 and 1669–1688 cm^{-1}), unordered structures (1642–1652 cm^{-1}), and turns (1659–1681 cm^{-1}). Curve fitting methodologies were used as previously reported.[43] Statistical analysis was performed using Benjamini, Krieger, and Yekutieli *t*-test, with $Q = 1\%$.

Protein Adsorption—Cell Culture: All cell lines were cultured at 37 °C in 5% CO_2 in Dulbecco's modified Eagle´s media (DMEM; Sigma), supplemented with 10% (v/v) FCS (Sigma), 4.5 g L^{-1} D-glucose, 2 × 10^{-3} M L-glutamine, and 100 units mL^{-1} penicillin and 100 units mL^{-1} streptomycin (Invitrogen).

MNP Delivery in Cell Culture: All particles used during the experiments were dextran-coated Nanomag-D MNPs (Fe_3O_4 core; 250 nm; Micromod, product code 09-02-252). Unless differently stated, MNPs used were COOH functionalized dextran-coated Nanomag-D MNPs. GET was chemically synthesized.

Cells were plated and incubated overnight until they reached 70–80% confluency. They were then treated, with nothing (media exchange), MNPs (50 μg mL^{-1}), and GET–MNPs (50 μg mL^{-1}, at 4 nmol GET mg^{-1} of MNPs unless otherwise specified). Particle delivery was done overnight unless otherwise stated. Particle delivery was normally performed in 10% FCS unless otherwise specified.

Heparin Competition: P21-8R (GET) was complexed at a low concentration (4 nmol mg^{-1} MNPs) to confirm the effect of heparin using MNPs unsaturated with complexed GET peptide. Before particle delivery, fresh media was replaced in the cells with increasing concentrations of heparin (0, 0.01, 0.1, 1, and 10 μg mL^{-1}). After 1 h incubation, cells were then treated with MNPs (50 μg per well) and GET–MNPs (4 nmol mg^{-1}). 24 h postdelivery, cells were collected for analysis (ICP-MS and Prussian Blue staining).

MNP Delivery in Plasma: Due to the nature of the dextran, coating of the particles concentration or precipitation of the MNPs was not possible without obtaining a significant degree of aggregation. This made it very challenging to efficiently coat the MNPs with plasma and obtain consistent size particles. Delivery of particles and characterization in 100% plasma presented another challenge in terms of cell viability, affecting the reproducibility of the delivery. To overcome these technical issues, fluorescently labeled BSA was used. Albumin represents ≈50% of plasma protein content and therefore can be used as an estimate of the loading capacity of MNPs.[73] Langmuir modeling of the kinetics (generating isotherms; Figure S14, Supporting Information) was used and the amount of plasma needed to saturate the MNPs was extrapolated. $S_{\max}$ (the saturating amount) for albumin coating of MNPs was calculated to be around 318 μg mg^{-1} (Table S7, Supporting Information). Taking the density of plasma as 1.025 g mL^{-1}, it was estimated that in order to saturate 50 μg MNPs (the amounts used for delivery), ≈31 μL (3.1% v/v) of a typical batch of human plasma was required. As Langmuir isotherm analyses are a simplified model of protein adsorption, the $S_{\max}$ value was used as a minimum approximation. For size, charge analysis, and in vitro delivery, 50 μL of plasma (5% v/v in 1 mL) per 50 μg of MNPs was used unless otherwise specified.

Cell Viability Assays: After treatment with MNPs, cells were incubated for 24 h at 37 °C with 5% CO_2. After 24 h, cells were trypsinized and diluted in Trypan Blue (1:1) for cell count. Percentage of cell viability was calculated based on the total number of viable cells for each group compared to the untreated control. Half the trypsinized cells were plated again. Proliferation was measured as the cumulative number of viable cells every 24 h for 7 days.

FIB-SEM: After overnight treatment with GET–MNPs, BV2 cells were fixed in 2% glutaraldehyde solution for 2 h at 4 °C. Cells were then washed in cacodylate buffer (pH 7.2) and treated with potassium ferrocyanide 2.5% osmium tetroxide 1% for 1 h at room temperature. Cells were dehydrated in increasing concentrations of acetone (30%, 50%, 70%, 90%, and 100%). Images were taken using a Dual-Beam (Nova NanoLab 200, FEI Company) equipped with a Ga^+ ion beam column, operating with a beam voltage of 30 kV and an ion current of 10 pA. SEM images were taken with an FEG column, working at 5–10 kV and electron currents between 50 and 98 pA. Sequential cross-sectioning of single BV2 cells was performed using the FIB and then SEM images were taken to assess the intracellular localization of MNPs.

TEM: After overnight treatment with GET–MNPs, NIH3t3 cells were fixed in 3% (w/v) glutaraldehyde in 0.1 M cacodylate buffer for 1 h and postfixed in 1% aqueous osmium tetroxide for 30 min. The samples were then dehydrated in a graded ethanol series and infiltrated with Transmit resin (TAAB, UK), and then allowed to polymerize for 48 h at 70 °C. Semithin sections were cut (0.5 μm), using a Reichert-Jung ultramicrotome, and stained with 2% toluidine blue. Ultrathin sections were cut (100 μm) using the same equipment and collected on copper grids, which were then contrasted using 50% methanol uranyl acetate and Reynolds lead citrate. Imaging was performed on a Tecnai 12 Biotwin TEM (FEI, USA) run at 100 kV.

Iron Qualitative Analyses and Subcellular Localization by Prussian Blue Staining: Cells were fixed for 20 min with 4% (w/v) paraformaldehyde (Sigma) at room temperature. Prussian Blue staining solution: potassium ferrocyanide (Sigma) was diluted in a solution of 2.5% (v/v) hydrochloric acid (HCl) in distilled H_2O to a final concentration of 25 mg mL^{-1} (Scientific Laboratory Supplies). Prussian Blue staining solution was added to the cells and incubated for 1 h. Stained cells were imaged using a Nikon Eclipse TS1000 light microscope.

Iron Quantification by Inductively Coupled Plasma Mass Spectrophotometry: MNPs were delivered as described above. After incubation overnight, the supernatant was removed and cells were washed twice with PBS. Cells were trypsinized and lysed in HCl 6 M, HNO_3 (65%) for 2 h at room temperature for the degradation of the particles in order to release the Fe content. Samples were then diluted

in water in order to achieve a final acid concentration of less than 2% (w/v). A calibration curve was also produced at MNPs concentrations up to 50 μg mL^{-1} to account for possible matrix effects.

Diluted solutions were analyzed by ICP-MS (Thermo Fisher Scientific iCAP-Q; Thermo Fisher Scientific, Bremen, Germany). Elemental analysis of diluted solutions was undertaken by ICP-MS (Thermo Fisher Scientific iCAP-Q and iCAP-TQ; Thermo Fisher Scientific, Bremen, Germany). Samples were introduced (flow rate 1.2 mL min^{-1}) from an autosampler (Cetac ASX-520) incorporating an ASXpress rapid uptake module through a perfluoroalkoxy (PFA) Microflow PFA-ST nebulizer (Thermo Fisher Scientific, Bremen, Germany). Sample processing was undertaken using Qtegra software (Thermo Fisher Scientific) utilizing external cross-calibration between pulse-counting and analogue detector modes when required. Internal standards were introduced to the sample stream on a separate line via the ASXpress unit and included Ge (10 μg L^{-1}), Rh (10 μg L^{-1}), and Ir (5 μg L^{-1}) in 2% trace analysis grade (Fisher Scientific, UK) HNO_3. Fe external calibration standard (Claritas-PPT grade CLMS-2 from SPEX Certiprep Inc., Metuchen, NJ, USA), in the range 0–100 μg L^{-1} (0, 20, 40, and 100 μg L^{-1}) was employed. Phosphorus, boron, and sulfur calibration utilized in-house standard solutions (KH_2PO_4, K_2SO_4, and H_3BO_3). A collision-cell (Q cell) using He with kinetic energy discrimination (He-cell) to remove polyatomic interferences was used to measure Fe. Sample processing was undertaken using Qtegra software (Thermo Fisher Scientific). Results were reported back in ppb (μg L^{-1}). Iron association per cell was calculated based on the doubling times of the respective cell lines to estimate total number of cells. Sidak's multiple comparisons test was used to determine significant differences between samples.

SDS-PAGE Analyses: For determination of plasma proteins adsorbed onto the particles (MNPs and GET–MNPs), SDS-PAGE using Novex 12.5% Tris-Glycine mini protein gel (Invitrogen) was used following the manufacturer's instructions. Gels were stained with Coomassie blue (Invitrogen) and destained before imaging.

LC-MS and Snapshot Proteomics: Human plasma was obtained from Sigma (pooled human blood). MNPs and GET–MNPs were incubated in plasma for 1 and 30 min at 37 °C. After incubation, particles were centrifuged (5 min at 14 000 × *g*) and separated from the plasma aided by a static field. Particles pellets were washed twice with PBS. Particles were then digested with trypsin and analyzed by liquid chromatography coupled with tandem mass spectrometry (LC-MS/MS) using either a 4000 Q-Trap (Applied Biosystems, Carlsbad, CA, USA) mass spectrometer.

Proteomics results were analyzed using Scaffold software. Key identification parameters were set to 95% protein threshold, minimum number of peptides 2, and peptide threshold of 95%. Quantitative analysis was done by NSAF. Proteins were then clustered based on size (molecular weight), isoelectric point, and protein family. Differential abundance of a protein was calculated as a function of protein relative abundance in nanoparticles/average of the relative abundance across all samples. *N* represents the number of independent experiments (each independent experiment was performed with a different plasma batch, with two experimental replicates per experiment).

Hematocompatibility Assays—Erythrocyte Aggregation: The impact of the GET–MNPs on erythrocyte aggregation and hemolysis were analyzed as described.[24] Briefly, human blood sample was purchased from NHS. Blood was transferred into tubes and centrifuged at 5000 × *g* for 5 min. The cell pellet was washed twice with PBS. To quantify aggregation, 6×10^5 erythrocytes were mixed to final concentrations of 100 μg mL^{-1} GET-MNPs (4 nmol mg^{-1}). After incubation under constant shaking at 37 °C for 5, 15, and 30 min, cell aggregation was evaluated using Nikon Eclipse TS1000 light microscope. As negative control for aggregation, erythrocytes were treated with either PBS or plasma alone.

Hematocompatibility Assays—Hemolysis: To assess the hemolytic activity of GET–MNPs, 6×10^6 erythrocytes were mixed to final concentrations of 100 μg mL^{-1} MNPs GET–MNPs (4 nmol mg^{-1}). Cells were also mixed with MNPs only (100 μg mL^{-1}) and GET only (0.4 nmol mL^{-1}). After incubation for 5, 15, and 30 min, samples were centrifuged at 5000 × *g* for 5 min. The supernatant was collected and hemoglobin content was analyzed by spectrophotometry at 544 nm (Infinite 200 PRO, TECAN). PBS and plasma were used as controls. Results were expressed as percentage lysis taking Triton-x 100 as complete lysis (100%).

Statistical Analysis: For in vitro studies, *n* represents the number of biological repeats. Technical replicates refer to experiments carried out with different passage cells but identical experimental conditions. Data were presented as mean ± s.d. Significant differences between test groups were analyzed by two-way ANOVA. *p* values <0.05 were considered statistically significant. Data were analyzed by Prism statistical analysis software (GraphPad v. 7.03).

Supporting Information

Supporting Information is available from the Wiley Online Library or from the author.

Acknowledgements

The research conducted in this study was funded by the European Research Council under the European Community's Seventh Framework Programme (FP7/2007–2013)/ERC grant agreement 227845. This work was supported by the Medical Research Council (grant number MR/K026682/1), the Engineering and Physical Sciences Research Council, and the Biotechnology and Biological Sciences Research Council, acknowledged by J.E.D. and K.M.S. for the UK Regenerative Medicine Platform Hub "Acellular Approaches for Therapeutic Delivery." L.A.B.F. acknowledges the studentship supported by the Engineering and Physical Sciences Research Council (EP/F500491/1) in the Centre of Doctoral Training in Regenerative Medicine. The authors are grateful to Dr. Robert Markus for assistance with confocal microscopy, Dr. Beatriz Sanz for assistance in preparing FIB-SEM samples, and Dr. Robert Layfield for assistance with the proteomics data.

Conflict of Interest

The authors declare no conflict of interest.

Author Contributions

L.A.B.F. and J.E.D. conceived and initiated the project; L.A.B.F., P.R., G.F.G., and J.E.D. designed the experiments; L.A.B.F., D.S., S.V.R., P.R., T.E.T., and G.F.G. conducted the experiments; K.M.S. and J.E.D. supervised the study; L.A.B.F. and J.E.D. wrote the manuscript; all authors approved the final manuscript.

Keywords

cell penetrating peptide (CPP), glycosaminoglycan-binding enhanced transduction (GET)-binding enhanced transduction, intracellular transduction, magnetic nanoparticles, protein corona

Received: June 23, 2020
Revised: August 6, 2020
Published online:

[1] J. J. Giner-Casares, M. Henriksen-Lacey, M. Coronado-Puchau, L. M. Liz-Marzán, *Mater. Today* **2016**, *19*, 19.

[2] K. Ulbrich, K. Holá, V. Šubr, A. Bakandritsos, J. Tuček, R. Zbořil, *Chem. Rev.* **2016**, *116*, 5338.
[3] R. Hergt, S. Dutz, R. Müller, M. Zeisberger, *J. Phys.: Condens. Matter* **2006**, *18*, S2919.
[4] R. Duncan, R. Gaspar, *Mol. Pharmaceutics* **2011**, *8*, 2101.
[5] R. Hergt, S. Dutz, R. Müller, M. Zeisberger, *J. Phys.: Condens. Matter* **2006**, *18*, S2919.
[6] J. M. Byrne, V. S. Coker, E. Cespedes, P. L. Wincott, D. J. Vaughan, R. A. D. Pattrick, G. van der Laan, E. Arenholz, F. , Tuna, M. Bencsik, J. R. Lloyd, N. D. Telling, *Adv. Funct. Mater.* **2014**, *24*, 2518.
[7] H. Markides, J. S. McLaren, A. J. El Haj, *Int. J. Biochem. Cell Biol.* **2015**, *69*, 162.
[8] H. Markides, M. Rotherham, A. J. El Haj, *J. Nanomater.* **2012**, *2012*, 614094.
[9] H. Markides, K. J. Newell, H. Rudorf, L. B. Ferreras, J. E. Dixon, R. H. Morris, M. Graves, J. Kaggie, F. Henson, A. J. El Haj, *Stem Cell Res. Ther.* **2019**, *10*, 25.
[10] C. Plank, O. Zelphati, O. Mykhaylyk, *Adv. Drug Delivery Rev.* **2011**, *63*, 1300.
[11] R. Hergt, S. Dutz, R. Müller, M. Zeisberger, *J. Phys.: Condens. Matter* **2006**, *18*, S2919.
[12] V. V. Mody, A. Cox, S. Shah, A. Singh, W. Bevins, H. Parihar, *Appl. Nanosci.* **2014**, *4*, 385.
[13] J. Riegl, J. A. Wells, P. G. Kyrtatos, A. N. Price, Q. A. Pankhurst, M. F. Lythgoe, *Biomaterials* **2010**, *31*, 5366.
[14] K. T. Al-Jamal, J. Bai, J. Tzu-Wen Wang, A. Protti, P. Southern, L. Bogart, H. Heidari, X. Li, A. Cakebread, D. Asker, W. T. Al-Jamal, A. Shah, S. Bals, J. Sosabowski, Q. A. Pankhurst, *Nano Lett.* **2016**, *16*, 5652.
[15] M. Muthana, A. J. Kennerley, R. Hughes, E. Fagnano, J. Richardson, M. Paul, C. Murdoch, F. Wright, C. Payne, M. F. Lythgoe, N. Farrow, J. Dobson, J. Conner, J. M. Wild, C. Lewis, *Nat. Commun.* **2015**, *6*, 8009.
[16] R. Singh, J. W. LillardJr., *Exp. Mol. Pathol.* **2009**, *86*, 215.
[17] K. Sharer, E. M. Shapiro, K. Sharer, S. Skrtic, A. P. Koretsky, *Magn. Reson. Med.* **2006**, *55*, 242.
[18] D. Wang, H. Wu, S. Z. F. Phua, G. Yang, W. Q. Lim, L. Gu, C. Qian, H. Wang, Z. Guo, H. Chen, Y. Zhao, *Nat. Commun.* **2020**, *11*, 357.
[19] A. Salvati, A. S. Pitek, M. P. Monopoli, K. Prapainop, F. B. Bombelli, D. R. Hristov, P. M. Kelly, C. Åberg, E. Mahon, K. A. Dawson, *Nat. Nanotechnol.* **2013**, *8*, 137.
[20] C. J. Cheng, G. T. Tietjen, J. K. Saucier-Sawyer, W. M. Saltzman, *Nat. Rev.* **2015**, *14*, 239.
[21] K. E. Sapsford, W. R. Algar, L. Berti, K. Boeneman Gemmill, B. J. Casey, E. Oh, M. H. Stewart, I. L. Medintz, *Chem. Rev.* **2013**, *113*, 1904.
[22] M. P. Monopoli, D. Walczyk, A. Campbell, G. Elia, I. Lynch, F. B. Bombelli, K. A. Dawson, *J. Am. Chem. Soc.* **2011**, *133*, 2525.
[23] L. Treuel, S. Brandholt, P. Maffre, S. Wiegele, L. Shang, G. U. Nienhaus, *ACS Nano* **2014**, *8*, 503.
[24] S. Tenzer, D. Docter, J. Kuharev, A. Musyanovych, V. Fetz, R. Hecht, F. Schlenk, D. Fischer, K. Kiouptsi, C. Reinhardt, K. Landfester, H. Schild, M. Maskos, S. K. Knauer, R. H. Stauber, *Nat. Nanotechnol.* **2013**, *8*, 772.
[25] C. C. Fleischer, C. K. Payne, *Acc. Chem. Res.* **2014**, *47*, 2651.
[26] A. Nandakumar, Y. Xing, R. R. Aranha, A. Faridi, A. Kakinen, I. Javed, K. Koppel, E. H. Pilkington, A. W. Purcell, T. P. Davis, P. Faridi, F. Ding, P. C. Ke, *Biomacromolecules* **2020**, *21*, 988.
[27] J. E. Dixon, G. Osman, G. E. Morris, H. Markides, M. Rotherham, Z. Bayoussef, A. J. El Haj, C. Denning, K. M. Shakesheff, *Proc. Natl. Acad. Sci. USA* **2016**, *113*, E291.
[28] G. Osman, J. Rodriguez, S. Y. Chan, J. Chisholm, G. Duncan, N. Kim, A. L. Tatler, K. M. Shakesheff, J. Hanes, J. S. Suk, J. E. Dixona, *J. Controlled Release* **2018**, *285*, 35.
[29] R. M. Raftery, D. P. Walsh, L. B. Ferreras, I. M. Castaño, G. Chen, M. LeMoine, G. Osman, K. M. Shakesheff, J. E. Dixon, F. J. O'Brien, *Biomaterials* **2019**, *216*, 119277.
[30] L. Thiagarajan, H. A. D. M. Abu-Awwad, J. E. Dixon, *Stem Cells Transl. Med.* **2017**, *6*, 2146.
[31] H. A. D. M. Abu-Awwad, L. Thiagarajan, J. E. Dixon, *Acta Biomater.* **2017**, *57*, 225.
[32] H. M. Eltaher, J. Yang, K. M. Shakesheff, J. E. Dixon, *Acta Biomater.* **2016**, *41*, 181.
[33] S. C. McBain, H. H. P. Yiu, A. El Haj, J. Dobson, *J. Mater. Chem.* **2007**, *17*, 2561.
[34] O. Mykhaylyk, A. Cherchenko, A. Ilkin, N. Dudchenko, V. Ruditsa, M. Novoseletz, Y.u. Zozulya, *J. Magn. Magn. Mater.* **2001**, *225*, 241.
[35] J. Estelrich, E. Escribano, J. Queralt, M. A. Busquets, *Int. J. Mol. Sci.* **2015**, *16*, 8070.
[36] I. Marcos-Campos, L. Asín, T. E. Torres, C. Marquina, A. Tres, M. R. Ibarra, G. F. Goya, *Nanotechnology* **2011**, *22*, 205101.
[37] J. Stetefeld, S. A. McKenna, T. R. Patel, *Biophys. Rev.* **2016**, *8*, 409.
[38] M. Rabe, D. Verdes, S. Seeger, *Adv. Colloid Interface Sci.* **2011**, *162*, 87.
[39] P. Roach, D. Farrar, C. C. Perry, *J. Am. Chem. Soc.* **2005**, *127*, 8168.
[40] L. Treuel, S. Brandholt, P. Maffre, S. Wiegele, L. Shang, G. U. Nienhaus, *ACS Nano* **2014**, *8*, 503.
[41] I. Amenabar, S. Poly, W. Nuansing, E. H. Hubrich, A. A. Govyadinov, F. Huth, R. Krutokhvostov, L. Zhang, M. Knez, J. Heberle, A. M. Bittner, R. Hillenbrand, *Nat. Commun.* **2013**, *4*, 2890.
[42] B. S. Kendrick, A. Dong, S. D. Allison, M. C. Manning, J. F. Carpenter, *J. Pharm. Sci.* **1996**, *85*, 155.
[43] P. Roach, D. Farrar, C. C. Perry, *J. Am. Chem. Soc.* **2006**, *128*, 3939.
[44] R. A. Latour, *J. Biomed. Mater. Res. Part A* **2015**, *103*, 949.
[45] C. M. Alves, R. L. Reis, J. A. Hunt, *J. R. Soc. Interface* **2010**, *7*, 1367.
[46] D. Coglitore, J. M. Janot, S. Balme, *Adv. Colloid Interface Sci.* **2019**, *270*, 278.
[47] A. A. A. Darwish, M. Rashad, H. A. Al-Aoh, *Dyes Pigm.* **2019**, *160*, 563.
[48] S. Rajput, C. U. Pittman, D. Mohan, *J. Colloid Interface Sci.* **2016**, *468*, 334.
[49] W. Cui, J. Li, Y. Zhang, H. Rong, W. Lu, L. Jiang, *Nanomedicine* **2012**, *8*, 46.
[50] N. Oh, J.-H. Park, *Int. J. Nanomed.* **2014**, *9*, 51.
[51] A. Albanese, W. C. W. Chan, *ACS Nano* **2011**, *5*, 5478.
[52] S. Console, C. Marty, C. García-Echeverría, R. Schwendener, K. Ballmer-Hofer, *J. Biol. Chem.* **2003**, *278*, 35109
[53] M. R. Birtwistle, B. N. Kholodenko, *Mol. Oncol.* **2010**, *3*, 308.
[54] A. Salvati, C. Aberg, T. dos Santos, J. Varela, P. Pinto, I. Lynch, K. A. Dawson, *Nanomedicine* **2011**, *7*, 818.
[55] S. L. Schmid, L. L. Carter, *J. Cell Biol.* **1989**, *111*, 2307.
[56] F. Mazuel, A. Espinosa, N. Luciani, M. Reffay, R. L. Borgne, L. Motte, K. Desboeufs, A. Michel, T. Pellegrino, Y. Lalatonne, C. Wilhelm, *ACS Nano* **2016**, *10*, 7627
[57] M. Tonigold, J. Simon, D. Estupiñán, M. Kokkinopoulou, R. J. U. Kintzel, A. Kaltbeitzel, P. Renz, M. P. Domogalla, K. Steinbrink, I. Lieberwirth, D. Crespy, K. Landfester, V. Mailänder, *Nat. Nanotechnol.* **2018**, *13*, 862.
[58] Z. Zhang, J. Guan, Z. Jiang, Y. Yang, J. Liu, W. Hua, Y. Mao, C. Li, W. Lu, J. Qian, C. Zhan, *Nat. Commun.* **2019**, *10*, 3561.
[59] H. J. Issaq, Z. Xiao, T. D. Veenstra, *Chem. Rev.* **2007**, *107*, 3601.
[60] M. Lundqvist, C. Augustsson, M. Lilja, K. Lundkvist, B. Dahlbäck, S. Linse, T. Cedervall, *PLoS One* **2017**, *12*, e0175871.
[61] V. Mirshafiee, R. Kim, M. Mahmoudi, M. L. Kraft, *Int. J. Biochem. Cell Biol.* **2016**, *75*, 188.
[62] C. Corbo, R. Molinaro, A. Parodi, N. E. T. Furman, F. Salvatore, E. Tasciotti, *Nanomedicine* **2016**, *11*, 81.
[63] C. D. Walkey, J. B. Olsen, F. Song, R. Liu, H. Guo, D. W. H. Olsen, Y. Cohen, A. Emili, W. C. W. Chan, *ACS Nano* **2014**, *8*, 2439.
[64] J. Simon, L. K. Müller, M. Kokkinopoulou, I. Lieberwirth, S. Morsbach, K. Landfester, V. Mailänder, *Nanoscale* **2018**, *10*, 10731.
[65] M. P. Monopoli, C. Åberg, A. Salvati, K. A. Dawson, *Nat. Nanotechnol.* **2012**, *7*, 779.

[66] S. Ritz, S. Schöttler, N. Kotman, G. Baier, A. Musyanovych, J. Kuharev, K. Landfester, H. Schild, O. Jahn, S. Tenzer, V. Mailänder, *Biomacromolecules* **2015**, *16*, 1311.
[67] L. Vroman, *Nature* **1962**, *196*, 476.
[68] M. A. Dobrovolskaia, D. R. Germolec, J. L. Weaver, *Nat. Nanotechnol.* **2009**, *4*, 411.
[69] J. D. Moyer, R. B. Nowak, N. E. Kim, S. K. Larkin, L. L. Peters, J. Hartwig, F. A. Kuypers, V. M. Fowler, *Blood* **2010**, *116*, 2590.
[70] M. Friebel, *J. Biomed. Opt.* **2010**, *15*, 055005.
[71] C. Wagner, P. Ste, S. Svetina, *C. R. Phys.* **2013**, *14*, 459.
[72] G. Kemmer, S. Keller, *Nat. Protoc.* **2010**, *5*, 267.
[73] A. Farrugia, *Transfus. Med. Rev.* **2010**, *24*, 53.